

Nitric acid uptake on subtropical cirrus cloud particles

P. J. Popp,^{1,2} R. S. Gao,³ T. P. Marcy,^{1,2} D. W. Fahey,^{1,2} P. K. Hudson,^{1,2} T. L. Thompson,¹ B. Kärcher,⁴ B. A. Ridley,⁵ A. J. Weinheimer,⁵ D. J. Knapp,⁵ D. D. Montzka,⁵ D. Baumgardner,⁶ T. J. Garrett,⁷ E. M. Weinstock,⁸ J. B. Smith,⁸ D. S. Sayres,⁸ J. V. Pittman,⁸ S. Dhaniala,^{9,10} T. P. Bui,¹¹ and M. J. Mahoney¹²

Received 16 October 2003; revised 9 January 2004; accepted 2 February 2004; published 17 March 2004.

[1] The redistribution of HNO₃ via uptake and sedimentation by cirrus cloud particles is considered an important term in the upper tropospheric budget of reactive nitrogen. Numerous cirrus cloud encounters by the NASA WB-57F high-altitude research aircraft during the Cirrus Regional Study of Tropical Anvils and Cirrus Layers-Florida Area Cirrus Experiment (CRYSTAL-FACE) were accompanied by the observation of condensed-phase HNO₃ with the NOAA chemical ionization mass spectrometer. The instrument measures HNO₃ with two independent channels of detection connected to separate forward and downward facing inlets that allow a determination of the amount of HNO₃ condensed on ice particles. Subtropical cirrus clouds, as indicated by the presence of ice particles, were observed coincident with condensed-phase HNO₃ at temperatures of 197–224 K and pressures of 122–224 hPa. Maximum levels of condensed-phase HNO₃ approached the gas-phase equivalent of 0.8 ppbv. Ice particle surface coverages as high as 1.4×10^{14} molecules cm⁻² were observed. A dissociative Langmuir adsorption model, when using an empirically derived HNO₃ adsorption enthalpy of -11.0 kcal mol⁻¹, effectively describes the observed molecular coverages to within a factor of 5. The percentage of total HNO₃ in the condensed phase ranged from near zero to 100% in the observed cirrus clouds. With volume-weighted mean particle diameters up to 700 μm and particle fall velocities up to 10 m s⁻¹, some observed clouds have significant potential to redistribute HNO₃ in the upper troposphere.

INDEX TERMS: 0305 Atmospheric Composition and Structure: Aerosols and particles (0345, 4801); 0320 Atmospheric Composition and Structure: Cloud physics and chemistry; 0322 Atmospheric Composition and Structure: Constituent sources and sinks;

KEYWORDS: cirrus clouds, nitric acid, uptake, ice particles

Citation: Popp, P. J., et al. (2004), Nitric acid uptake on subtropical cirrus cloud particles, *J. Geophys. Res.*, 109, D06302, doi:10.1029/2003JD004255.

¹Cooperative Institute for Research in Environmental Sciences, University of Colorado, Boulder, Colorado, USA.

²Also at Aeronomy Laboratory, National Oceanic and Atmospheric Administration, Boulder, Colorado, USA.

³Aeronomy Laboratory, National Oceanic and Atmospheric Administration, Boulder, Colorado, USA.

⁴Institut für Physik der Atmosphäre, Deutsches Zentrum für Luft- und Raumfahrt Institut für Physik der Atmosphäre, Wessling, Germany.

⁵Atmospheric Chemistry Division, National Center for Atmospheric Research, Boulder, Colorado, USA.

⁶Universidad Nacional Autónoma de México, Centro de Ciencias de la Atmósfera, Ciudad Universitaria, México City, México.

⁷Department of Meteorology, University of Utah, Salt Lake City, Utah, USA.

⁸Atmospheric Research Project, Harvard University, Cambridge, Massachusetts, USA.

⁹Division of Geology and Planetary Sciences, California Institute of Technology, Pasadena, California, USA.

¹⁰Now at Department of Mechanical and Aeronautical Engineering, Clarkson University, Potsdam, New York, USA.

¹¹NASA Ames Research Center, Moffett Field, California, USA.

¹²Jet Propulsion Laboratory, California Institute of Technology, Pasadena, California, USA.

1. Introduction

[2] Cirrus clouds are ubiquitous throughout the upper troposphere (UT) and can cover as much as 40% of Earth's surface [Liao *et al.*, 1995; Jin *et al.*, 1996; Wang *et al.*, 1996; Wylie and Menzel, 1999]. Composed of ice crystals [Lynch, 2002], cirrus clouds are known to play a complex and significant role in the global radiation budget [Liou, 1986]. Cirrus clouds can be formed in situ in the UT [Kärcher, 2002], as a result of synoptic weather disturbances, or in the anvil outflow at the top of cumulonimbus clouds [Sassen, 2002]. Tropical cirrus clouds around the peak convective detrainment level are formed primarily via the latter mechanism, and can reach altitudes of up to 18 km when produced in deep convective systems. The broad lateral and vertical extent of anvil cirrus clouds produced in the tropics is expected to exert a greater influence on Earth's climate system than midlatitude cirrus [Heymsfield and McFarquhar, 2002]. Owing to the high altitudes and often-remote locations of tropical cirrus, however, comprehensive in situ measurements of these clouds have been limited.

[3] Model simulations by *Lawrence and Crutzen* [1998] suggest that the uptake and gravitational redistribution of nitric acid (HNO_3) by cirrus cloud particles may represent a significant sink of HNO_3 in the UT. Nitric acid serves as a primary reservoir species for nitrogen oxides (NO_x) [*Neuman et al.*, 2001], which are directly involved in the photochemical production of tropospheric ozone [*Jaeglé et al.*, 1998]. Model studies of cirrus-processed air have demonstrated that the sedimentary removal of HNO_3 from the UT can effect strong local reductions in NO_x , with the consequence of significant reductions in the net ozone production rate [*Meier and Hendricks*, 2002]. Since ozone is known to be an effective greenhouse gas in the troposphere [*Albritton et al.*, 2001], particularly near the tropopause [*Lacis et al.*, 1990], understanding the uptake and redistribution of HNO_3 by cirrus cloud particles may be important in assessing the contribution of cirrus clouds to the radiative forcing of climate change.

[4] A number of laboratory studies have investigated the uptake of HNO_3 on ice surfaces at temperatures typical of the UT. Experiments performed by *Zondlo et al.* [1997] on vapor-deposited ice films at 211 K resulted in observed HNO_3 surface coverages of 1.5×10^{15} molecules cm^{-2} . A series of similar experiments reported by *Hudson et al.* [2002] at an HNO_3 pressure ($P(\text{HNO}_3)$) of 1.1×10^{-6} hPa indicated a negative temperature dependence to the observed uptake, with coverages of 1.1×10^{14} to 5.9×10^{13} molecules cm^{-2} over a temperature range of 214–220 K. Uptake studies performed on ice films by *Abbatt* [1997] yielded coverages of up to 2.9×10^{14} molecules cm^{-2} at temperatures as low as 208 K, with no apparent dependency on $P(\text{HNO}_3)$ values over the range 1.7×10^{-7} to 4.1×10^{-6} hPa. *Hynes et al.* [2002] reported comparable coverages using a similar technique, although they observed coverages increasing by factor of 2 over a nearly 10-fold increase in $P(\text{HNO}_3)$, from 5.0×10^{-7} to 3.0×10^{-6} hPa. A laboratory study of HNO_3 uptake on nebulized half-micron diameter ice particles at 230 K yielded coverages similar to those observed on the ice films (1.2×10^{14} molecules cm^{-2}), although these experiments were performed at the relatively high $P(\text{HNO}_3)$ of 7×10^{-6} hPa [*Arora et al.*, 1999]. There has not yet been an extensive laboratory study of HNO_3 uptake on ice surfaces performed at $P(\text{HNO}_3)$ values typical of the UT ($<2.0 \times 10^{-7}$ hPa).

[5] Prior field studies of HNO_3 uptake on cirrus cloud particles have been made at mid and high latitudes. Measurements of total reactive nitrogen ($\text{NO}_y = \text{NO} + \text{NO}_2 + 2\text{N}_2\text{O}_5 + \text{HNO}_3 + \dots$) in a mountain wave cloud over the continental United States reported by *Weinheimer et al.* [1998] indicated that levels of condensed NO_y in the cloud approached 20% of total NO_y . Surface coverages on the wave cloud ice particles were calculated to be as high as 2.5×10^{13} molecules cm^{-2} [*Hudson et al.*, 2002]. Measurements of condensed-phase NO_y in cirrus layers in the Arctic UT by *Kondo et al.* [2003] yielded HNO_3 coverages as high as 1.6×10^{14} molecules cm^{-2} at temperatures of approximately 200 K, with coverages decreasing at warmer temperatures. *Meilinger et al.* [1999] conducted similar measurements in Arctic cirrus clouds at 196 K and reported coverages of only 1×10^{13} molecules cm^{-2} . An extensive dataset of measurements made at midlatitudes revealed median levels of condensed NO_y (assumed to be HNO_3)

in the Northern Hemisphere of 3.6×10^{12} molecules cm^{-2} to be greater than twice that observed in the Southern Hemisphere [*Ziereis et al.*, 2004].

[6] We report here an extensive dataset of in situ measurements, including gas- and condensed-phase HNO_3 and ice particle surface area density (SAD), obtained in subtropical in situ and anvil cirrus clouds. These measurements were conducted onboard the NASA WB-57F high-altitude research aircraft as part of the Cirrus Regional Study of Tropical Anvils and Cirrus Layers Florida Area Cirrus Experiment (CRYSTAL-FACE) mission. The data are used here to assess the uptake of HNO_3 by subtropical cirrus cloud particles and explore the partitioning of HNO_3 between the gas and ice particle phases in cirrus clouds.

2. Instrumentation

[7] This study utilizes data from a number of in situ instruments onboard the NASA WB-57F aircraft. Gas-phase and condensed-phase HNO_3 measurements made by chemical ionization mass spectrometry are described in more detail below. Particle size distribution and number density measurements made by the Cloud, Aerosol and Precipitation Spectrometer (CAPS) were used to derive SAD and volume-weighted mean diameter (VMD) for ice particles in the size range between 0.35–1550 μm [*Baumgardner et al.*, 2001]. Note that all particle sizes cited herein refer to particle diameter, and not radius. A second, independent measurement of SAD was provided by the Cloud Integrating Nephelometer (CIN) [*Gerber et al.*, 2000]. Ice water content (IWC) and water (H_2O) vapor were measured by the Harvard University Lyman- α hygrometer [*Weinstock et al.*, 1994; E. M. Weinstock et al., manuscript in preparation, 2004]. Nitric oxide (NO) and total reactive nitrogen (NO_y) were measured by catalytic reduction and chemiluminescence (A. J. Weinheimer et al., manuscript in preparation, 2004). Ambient temperature and pressure, and WB-57F true air speed were measured by the Meteorological Measurement System (MMS) [*Scott et al.*, 1990]. The precision and accuracy of these measurements are summarized in Table 1. Tropopause height was measured by the microwave temperature profiler (MTP) [*Denning et al.*, 1989].

[8] HNO_3 was measured using the NOAA chemical ionization mass spectrometer (CIMS) located in the third pallet position of the NASA WB-57F aircraft. This instrument measures HNO_3 with an accuracy of $\pm 20\%$ and precision of 30 pptv (1σ , 10-s averages), and has been described in detail elsewhere [*Neuman et al.*, 2000]. Prior to CRYSTAL-FACE, the NOAA CIMS was modified by the addition of a second independent channel for the measurement of HNO_3 and the relocation of the original sample inlet on the CIMS inlet pylon (Figure 1). The two CIMS channels are designed to provide identical measurements of gas-phase HNO_3 . Owing to differences in the particle sampling efficiencies of the two inlets, however, the two channels have different sensitivity to condensed-phase HNO_3 . When sampling in cirrus clouds, the forward facing front inlet samples both gas-phase HNO_3 and any HNO_3 condensed on the cirrus particles. The downward facing bottom inlet samples primarily gas-phase HNO_3 because the plane of the sampling orifice is parallel to the direction of flow over the inlet, which is set by the flow straightener.

Table 1. Measurement Details

Measurement	Institution	Precision ^a	Accuracy	Reference
HNO ₃	NOAA Aeronomy Lab	30 pptv, 10 pptv ^b	±20%	<i>Neuman et al.</i> [2001]
SAD-CAPS	Univ. Nacional Autonoma de Mexico	-	±50%	<i>Baumgardner et al.</i> [2001]
SAD-CIN	University of Utah	-	±15%	<i>Gerber et al.</i> [2000]
IWC	Harvard University	0.7 ppmv	±17%	<i>E. M. Weinstock et al.</i> (manuscript in preparation, 2004)
Water vapor	Harvard University	0.5 ppmv	±5%	<i>Weinstock et al.</i> [1994]
NO	NCAR	5 pptv	±6%	<i>A. J. Weinheimer et al.</i> (manuscript in preparation, 2004)
NO _y	NCAR	8 pptv	±12%	<i>A. J. Weinheimer et al.</i> (manuscript in preparation, 2004)
Temperature	NASA Ames	0.01 K	±0.3 K	<i>Scott et al.</i> [1990]
Pressure	NASA Ames	0.1 hPa	±0.3 hPa	<i>Scott et al.</i> [1990]
True air speed	NASA Ames	0.1 m s ⁻¹	±1 m s ⁻¹	<i>Scott et al.</i> [1990]

^aPrecision values are reported for 10-s averages.

^b10 pptv is the precision for condensed-phase HNO₃.

Semiempirical calculations indicate that approximately 50% of 0.1 μm particles and greater than 90% of 1 μm and larger particles are inertially stripped from the air sampled by the bottom inlet [Vincent *et al.*, 1986]. Calculations further suggest that ice particles greater than 10 μm in diameter (typical of cirrus clouds observed during CRYSTAL-FACE) are almost entirely removed from the sampled air. Thus, for most of the cirrus clouds sampled, the HNO₃ from the

bottom inlet is taken to be a measure of the gas-phase HNO₃ abundance.

[9] The conclusion that ice particles greater than approximately 1 μm are inertially separated from air sampled by the bottom inlet is further supported by measurements made in the contrail of the WB-57F during CRYSTAL-FACE. The contrail contained ice particles with high number densities (100–200 cm⁻³) and volume-weighted mean

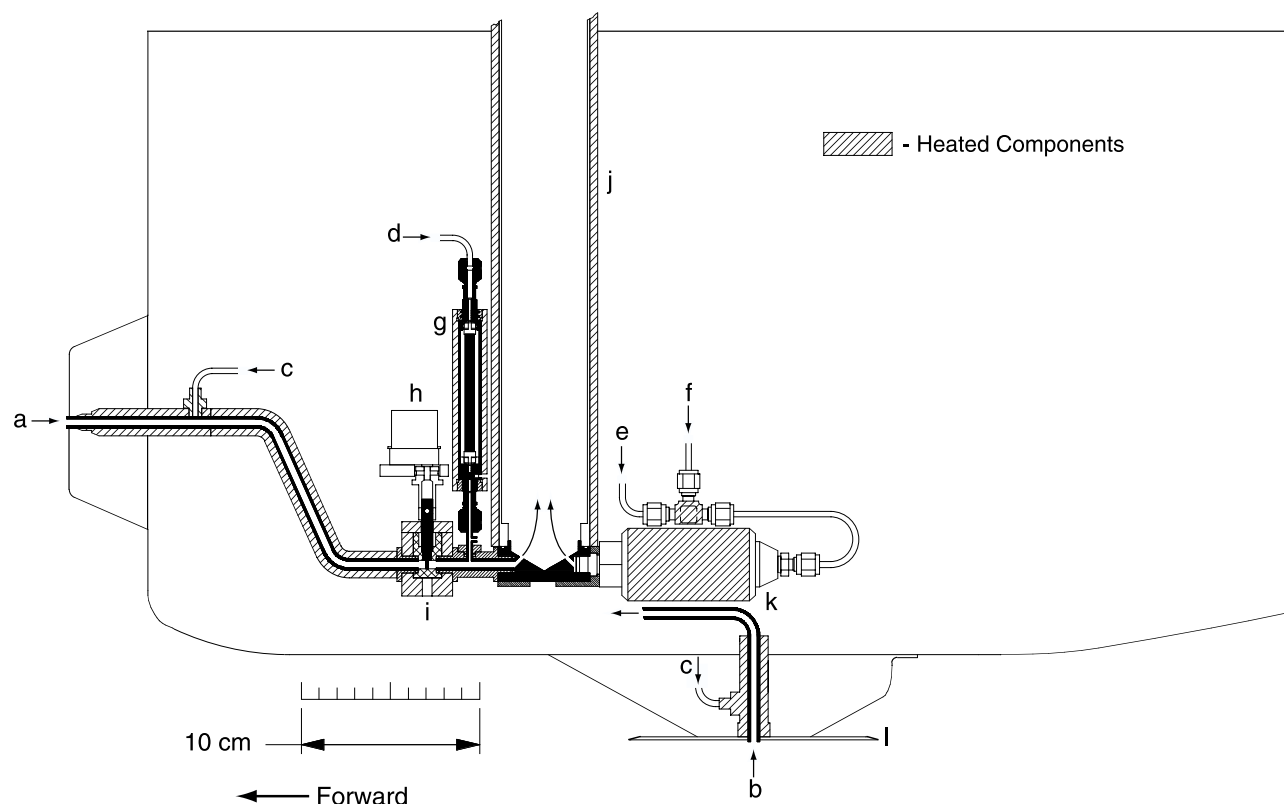


Figure 1. Schematic diagram of the NOAA CIMS inlet pylon. Labeled components are as follows: (a) front channel inlet, (b) bottom channel inlet, (c) zero gas addition, (d) calibration gas addition, (e) reagent gas carrier addition, (f) reagent gas addition, (g) HNO₃ permeation cell (calibration standard), (h) flow control valve motor, (i) flow control valve body, (j) flow tube, (k) ion source, and (l) flow straightener. For clarity, complete components are shown only for the front channel. Inlet lines are constructed of TeflonTM tubing (6.4 mm outside diameter, 4.0 mm inside diameter), heated to temperatures of 40°C (bottom channel inlet) and 48°C (front channel inlet) to avoid wall losses. The higher temperature of the front inlet ensures that ice particles entering the inlet evaporate upon impaction with the tubing wall. The operating principles of the NOAA CIMS instrument have been described in detail by *Neuman et al.* [2000].

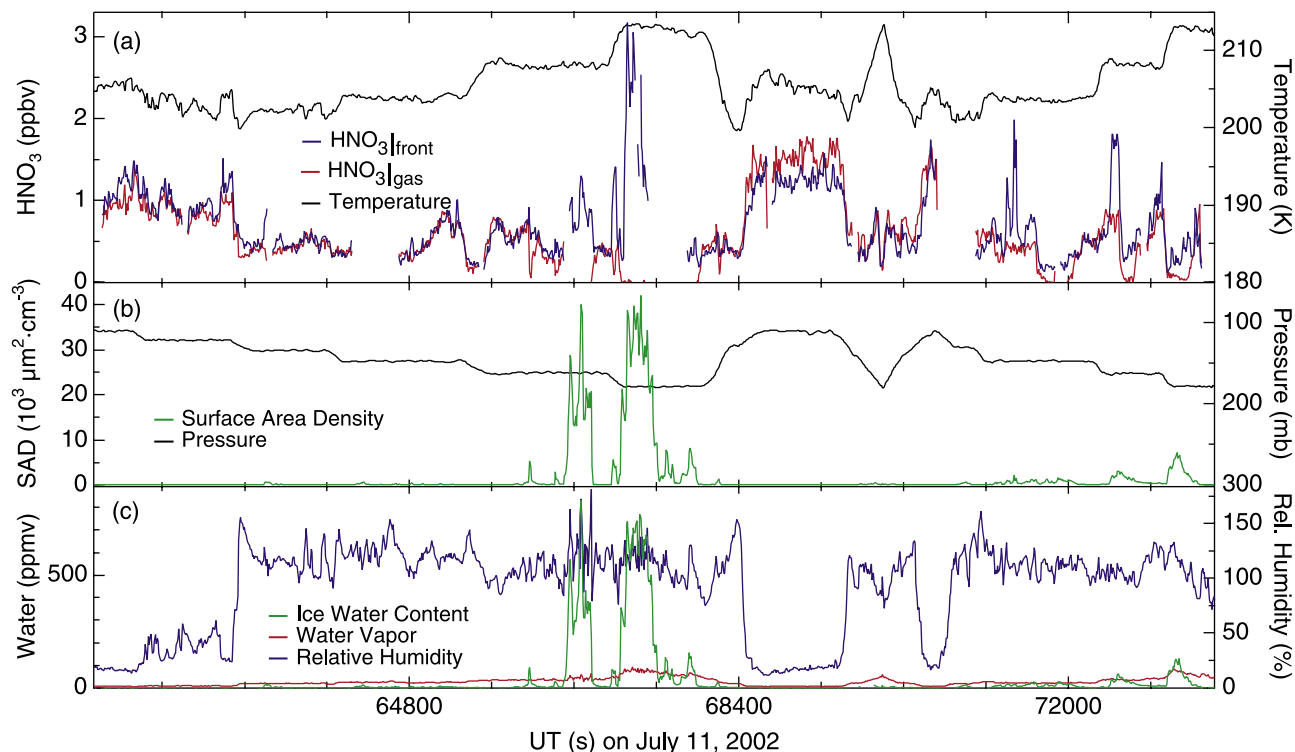


Figure 2. Time series measurements of the HNO_3 mixing ratio observed from the front and bottom CIMS channels ($\text{HNO}_3|_{\text{front}}$ and $\text{HNO}_3|_{\text{gas}}$, respectively,) on the flight of 11 July 2002. Note that values of $\text{HNO}_3|_{\text{front}}$ do not include a correction for particle oversampling in the front channel inlet. Discontinuities in the time series result from CIMS instrument calibrations and other housekeeping procedures. Also shown are SAD, IWC, water vapor, relative humidity (with respect to ice), and ambient temperature and pressure. All data are represented as 10-s averages. Minor divisions on the horizontal scale represent 15 min (or approximately 150 km) of flight.

diameters on the order of $2\ \mu\text{m}$ [Gao *et al.*, 2003]. HNO_3 was present in the contrail because of mixing between the exhaust gases and ambient air containing approximately 0.4 ppbv HNO_3 . Measurements in the contrail as soon as 4 min after formation indicated a difference between the front and bottom CIMS channels. The minimum signal from the bottom channel was near zero inside the contrail. This low HNO_3 signal is consistent with the removal of gas-phase HNO_3 by uptake onto the $2\text{-}\mu\text{m}$ ice particles in the contrail, and the inertial stripping of these particles from the bottom inlet sample flow. As expected, a simultaneous increase in HNO_3 above ambient values occurred in the front CIMS channel, which does not discriminate against $2\ \mu\text{m}$ particles. If the bottom CIMS inlet sampled $2\ \mu\text{m}$ particles with any significant efficiency, HNO_3 observed in the bottom channel during the contrail intercept would not be significantly lower than the ambient values immediately outside the contrail.

[10] The front CIMS inlet samples subisokinetically, meaning the sample air velocity inside the inlet (U) is less than the WB-57F true air speed (U_0) of $140\text{--}200\ \text{m s}^{-1}$ at sampling altitudes. As a result, cirrus cloud particle number densities in the sampled air stream are inertially enhanced relative to those in the ambient air. A computational fluid dynamics program (Fluent Inc., New Hampshire) was used to estimate particle enhancement factors (EF) in the front inlet by simulating the flow field and particle trajectories

around a two-dimensional horizontal cross section of the CIMS pylon and inlet structure (Figure 1). The value of EF is near unity for small particles ($<0.1\ \mu\text{m}$) and increases with particle size, as found for similar configurations [Northway *et al.*, 2002]. For particles larger than approximately $10\ \mu\text{m}$ in diameter, typical of cirrus cloud ice particles sampled during CRYSTAL-FACE, EF for the front inlet approaches the maximum value of U_0/U . Since both CIMS channels sample at a constant mass flow of 1.85 standard liters per minute (slpm), U , and therefore, EF , are dependent upon the ambient temperature and pressure. Under typical WB-57F sampling conditions during CRYSTAL-FACE (temperature = $213\ \text{K}$, pressure = $170\ \text{hPa}$, $U_0 = 200\ \text{m s}^{-1}$), EF has a maximum value of approximately 16.

[11] Cirrus cloud particles entering the front CIMS inlet travel through a 20 cm length of TeflonTM tubing (6.4 mm outside diameter, 4.0 mm inside diameter) upstream of the CIMS flow control valve and flow tube (Figure 1). The use of TeflonTM sample lines ensures that HNO_3 will not readily absorb on the inlet surfaces [Neuman *et al.*, 1999]. This tubing, which is heated to 48°C in flight, has two bends to help ensure that large particles entering the inlet will impact on the tubing walls and subsequently evaporate prior to reaching the flow control valve. Particles with diameters greater than approximately $20\ \mu\text{m}$ have large enough stopping distances at the freestream velocity that they

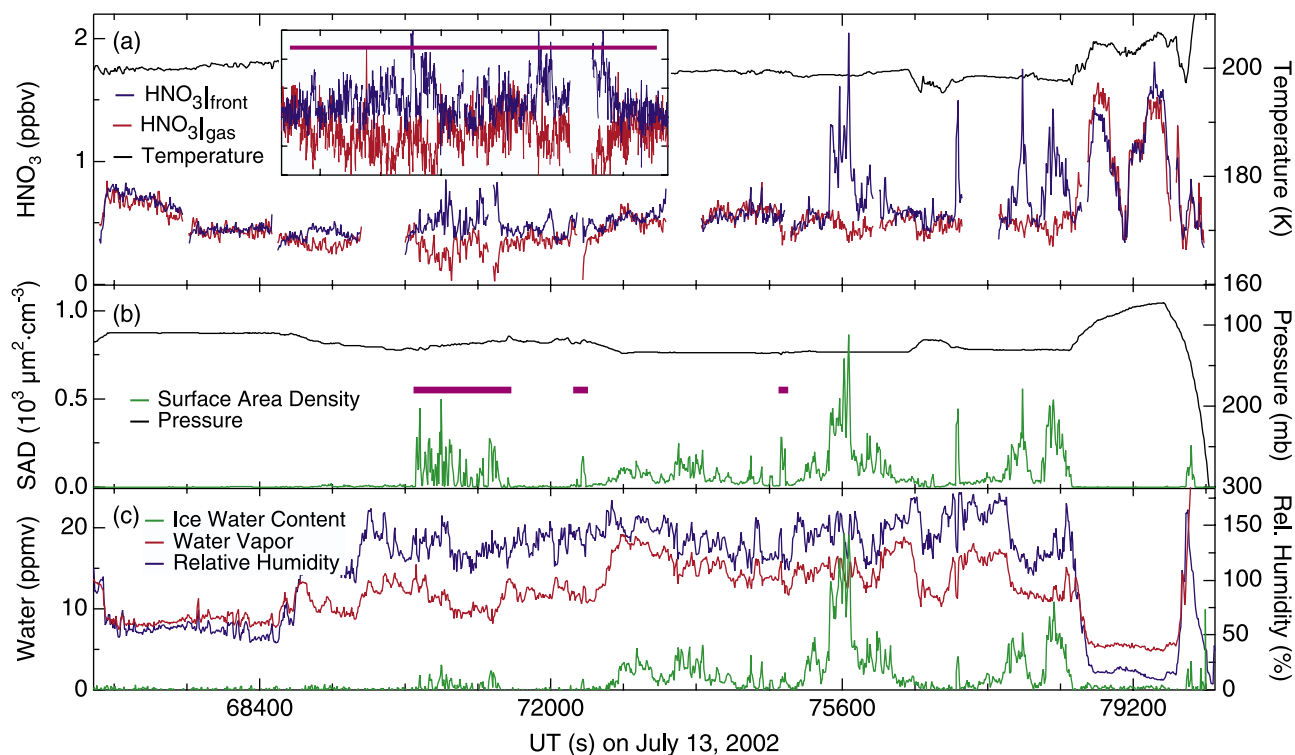


Figure 3. Same as Figure 2, for the flight on 13 July 2002. Purple bars in Figure 3b represent 3 flight segments in which cirrus clouds formed in the contrail of the WB-57F were observed. The inset in Figure 3a shows 1-s averages of $\text{HNO}_3|_{\text{front}}$ and $\text{HNO}_3|_{\text{gas}}$ during the first contrail intercept. The purple bar in the inset represents the same time period as the first purple bar in Figure 3b. The vertical scale on the inset panel is 0 to 1 ppbv. Measurements of $\text{HNO}_3|_{\text{front}}$ and $\text{HNO}_3|_{\text{gas}}$ are incomplete during the second and third contrail intercepts due to instrument housekeeping procedures.

impact at the first bend. Some particles that do not fully evaporate will impact in the body of the flow control valve or the flow tube entrance. HNO_3 condensed on the particle surfaces is liberated to the gas phase early in the evaporation process and measured as a gas-phase equivalent volume mixing ratio. The HNO_3 mixing ratio measured by the front CIMS channel, therefore, represents the sum of the gas- and the condensed-phase values, with the condensed-phase component enhanced by the value of EF .

3. Observations

[12] Condensed-phase HNO_3 was observed coincident with cirrus cloud observations on 4 WB-57F science flights conducted as part of CRYSTAL-FACE. These flights originated and terminated at the United States Naval Air Facility, Key West (24.6°N, 81.7°W) in Florida on 11, 13, 19, and 21 July 2002. Time series data of HNO_3 mixing ratios observed from the front and bottom CIMS channels ($\text{HNO}_3|_{\text{front}}$ and $\text{HNO}_3|_{\text{gas}}$, respectively), as well as particle SAD, IWC (represented as a gas-phase equivalent volume mixing ratio) and meteorological parameters are shown for 11, 13, 19, and 21 July in Figures 2–5, respectively. The presence of cirrus cloud particles is indicated by increases in SAD and IWC above background values. The presence of condensed-phase HNO_3 in a flight segment is indicated by $\text{HNO}_3|_{\text{front}}$ values that are significantly greater than $\text{HNO}_3|_{\text{gas}}$ values. Flight segments identified by purple bars

in panel (b) for 13 July (Figure 3) and 19 July (Figure 4) represent the observation of contrail cirrus clouds. As stated previously, these clouds are characterized by having high particle number densities with volume-weighted mean diameters typically much lower than cirrus clouds formed by natural processes. Owing to the uncertainties in the SAD measurements in the contrail-formed cirrus clouds and in the value of EF for particles in this size range, these clouds are not considered in the data analysis presented here.

[13] Cirrus clouds were observed from the WB-57F at pressures between 122 hPa and 224 hPa during the flights of 11, 13, 19, and 21 July, corresponding to pressure altitudes between 11 km and 15 km (Figures 2–5). These clouds were observed at temperatures between 197 K and 224 K. Figures 2–5 show the strong temporal correlation of $(\text{HNO}_3|_{\text{front}} - \text{HNO}_3|_{\text{gas}})$ with both SAD and IWC in cirrus clouds, with $\text{HNO}_3|_{\text{gas}}$ approaching zero during a number of cirrus events. Outside of clouds, measured values of $\text{HNO}_3|_{\text{front}}$ and $\text{HNO}_3|_{\text{gas}}$ generally agree well (with an overall correlation coefficient, r , of 0.92). However, some periods in Figures 2–5 show offsets between the two channels that are best explained as changes in the inlet line surfaces during the flight. Figure 4 also indicates elevated values of relative humidity (with respect to ice) during a number of cirrus cloud encounters, as described by Gao *et al.* [2003].

[14] Condensed-phase HNO_3 , proportional to the difference between the values of $\text{HNO}_3|_{\text{front}}$ and $\text{HNO}_3|_{\text{gas}}$, was

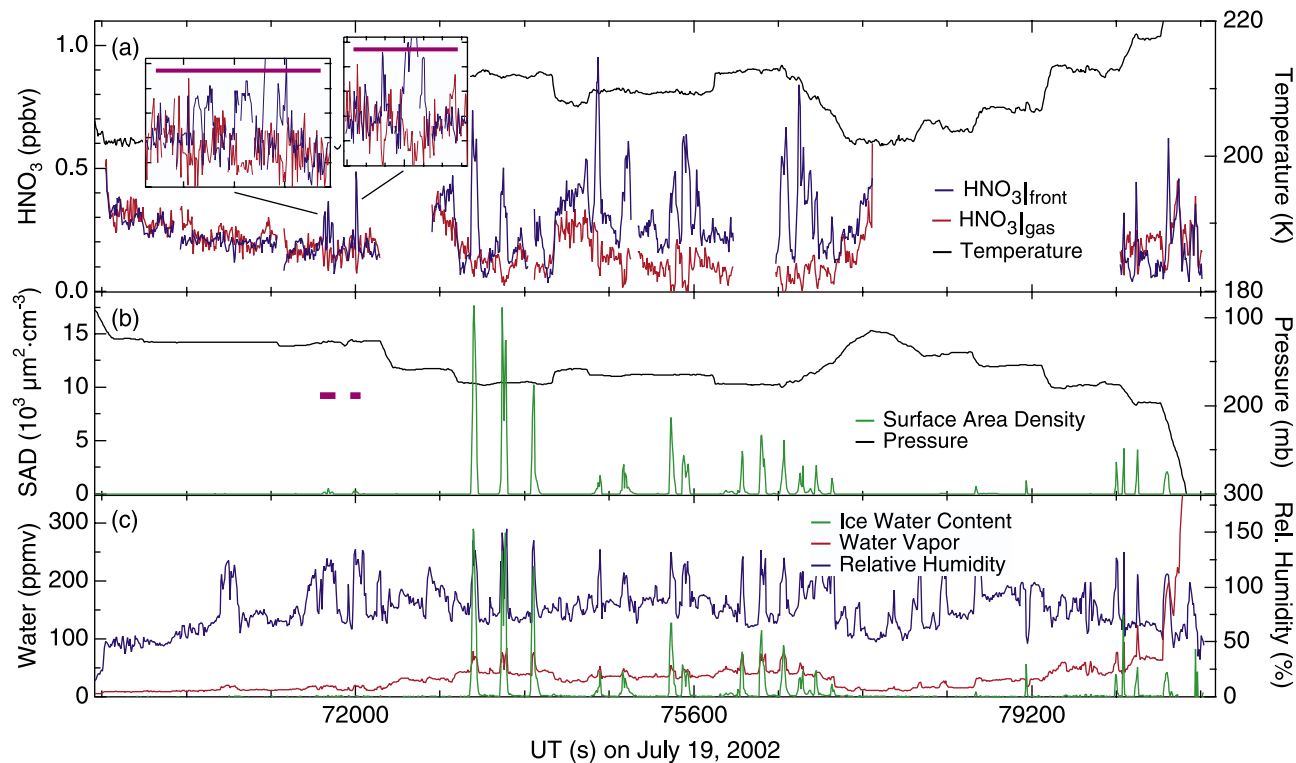


Figure 4. Same as Figure 2, for the flight on 19 July 2002. Purple bars in Figure 4b represent 2 flight segments in which cirrus clouds formed in the contrail of the WB-57F were observed. The insets in Figure 4a show 1-s averages of $\text{HNO}_3|_{\text{front}}$ and $\text{HNO}_3|_{\text{gas}}$ during the two contrail intercepts. The purple bars in the first and second insets represent the same time periods as the first and second purple bars in Figure 4b. The vertical scale on the inset panels is 0–0.5 ppbv.

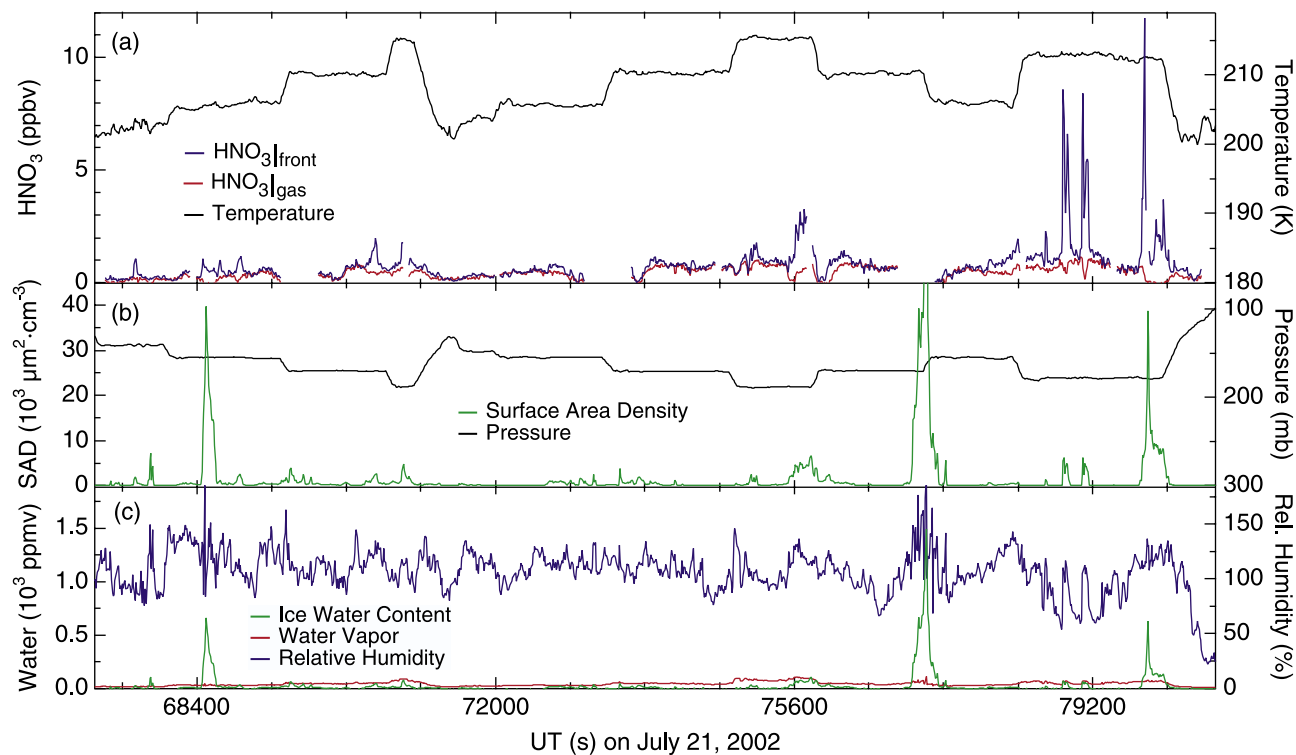


Figure 5. Same as Figure 2, for the flight on 21 July 2002.

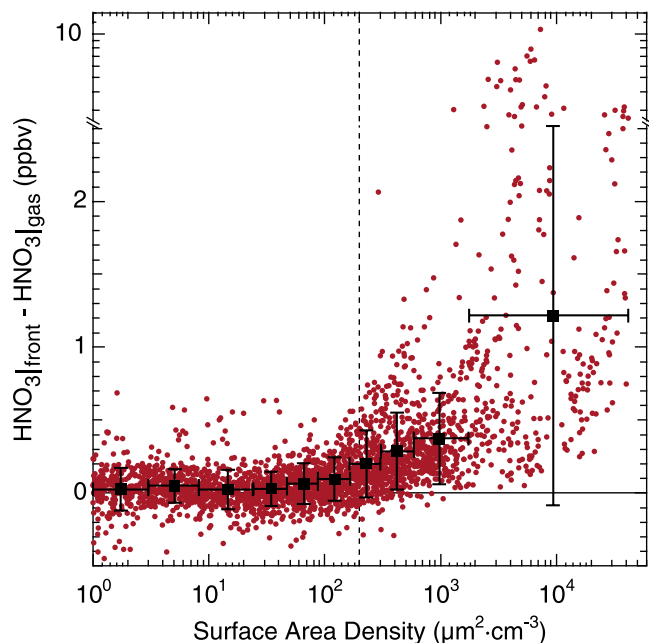


Figure 6. ($\text{HNO}_3|_{\text{front}} - \text{HNO}_3|_{\text{gas}}$) versus SAD for the flights of 11, 13, 19, and 21 July 2002. Values of ($\text{HNO}_3|_{\text{front}} - \text{HNO}_3|_{\text{gas}}$) are proportional but not equal to condensed-phase HNO_3 ($\text{HNO}_3|_{\text{con}}$) because they do not include a correction for particle oversampling in the front channel inlet. Red circles represent 10-s averages and black squares represent mean values of the 10-s data grouped into deciles. Vertical bars represent the standard deviation about the mean value in each decile, and horizontal bars indicate the upper and lower boundaries of each decile. Note that the vertical axis is shown with a logarithmic scale at values greater than 2.5. The dashed vertical line at the SAD of $200 \mu\text{m}^2 \text{cm}^{-3}$ represents the lower limit chosen here to represent measurements made in cirrus clouds.

observed primarily at SADs greater than $200 \mu\text{m}^2 \text{cm}^{-3}$ during CRYSTAL-FACE (Figure 6). Note that for the values of ($\text{HNO}_3|_{\text{front}} - \text{HNO}_3|_{\text{gas}}$) shown in Figure 6, $\text{HNO}_3|_{\text{front}}$ is not corrected for particle oversampling. Values of ($\text{HNO}_3|_{\text{front}} - \text{HNO}_3|_{\text{gas}}$) at SADs less than $200 \mu\text{m}^2 \text{cm}^{-3}$ are near the detection limit and highly variable due to CIMS instrument noise. In the analyses presented here, observations at SADs greater than $200 \mu\text{m}^2 \text{cm}^{-3}$ are selected to represent measurements made in cirrus clouds (shown by the dashed line in Figure 6).

3.1. Quantifying Condensed-Phase HNO_3

[15] As stated previously, $\text{HNO}_3|_{\text{front}}$ represents the sum of gas-phase and condensed-phase HNO_3 , with the condensed-phase component enhanced by the value of EF . The amount of HNO_3 condensed on cirrus cloud particles ($\text{HNO}_3|_{\text{con}}$) can therefore be calculated according to equation (1),

$$\text{HNO}_3|_{\text{con}} = \frac{\text{HNO}_3|_{\text{front}} - \text{HNO}_3|_{\text{gas}}}{EF}, \quad (1)$$

where $\text{HNO}_3|_{\text{con}}$ is reported as a gas-phase equivalent volume mixing ratio with a precision of 10 pptv (1σ , 10-s averages). The use of equation (1) in calculating $\text{HNO}_3|_{\text{con}}$ is illustrated in Figure 7 for a cirrus cloud encounter by the WB-57F on 13 July 2002. Increases in SAD and IWC

during this cloud event are accompanied by an increase in $\text{HNO}_3|_{\text{front}}$ above the gas-phase value of approximately 0.5 ppbv (Figures 7a, 7d, and 7e). Accounting for the particle enhancement factor of approximately 13.7 using equation (1), maximum values of $\text{HNO}_3|_{\text{con}}$ during this cloud event approached 0.1 ppbv (Figures 7b and 7c). It should be noted here that calculated values of $\text{HNO}_3|_{\text{con}}$ in cirrus clouds are not always consistent with the observed decreases in $\text{HNO}_3|_{\text{gas}}$ that result from HNO_3 uptake. Quantitative agreement between $\text{HNO}_3|_{\text{con}}$ and deficits in $\text{HNO}_3|_{\text{gas}}$ can only occur if the cloud particles are sampled in the same air mass in which uptake occurred. Owing to gravitational settling, however, cirrus particles may sediment into air masses that may be more or less depleted in gas-phase HNO_3 at the time of sampling.

3.2. Cirrus Cloud Particle Measurements

[16] Cirrus cloud particle SAD was derived from measurements provided by both the CAPS and CIN instruments

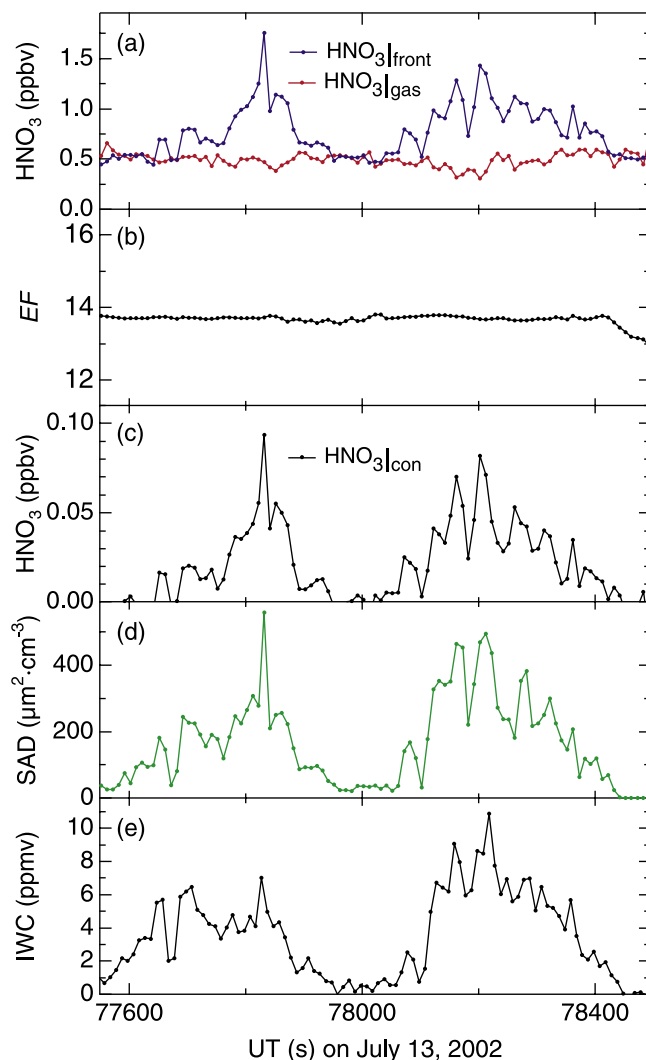


Figure 7. Calculation of $\text{HNO}_3|_{\text{con}}$ for a cirrus cloud encounter by the NASA WB-57F on 13 July 2002, showing (a) $\text{HNO}_3|_{\text{front}}$ and $\text{HNO}_3|_{\text{gas}}$, (b) EF , (c) $\text{HNO}_3|_{\text{con}}$, (d) SAD, and (e) IWC. All data are shown as 10-s averages. The horizontal axis spans approximately 16 min and 180 km of flight.

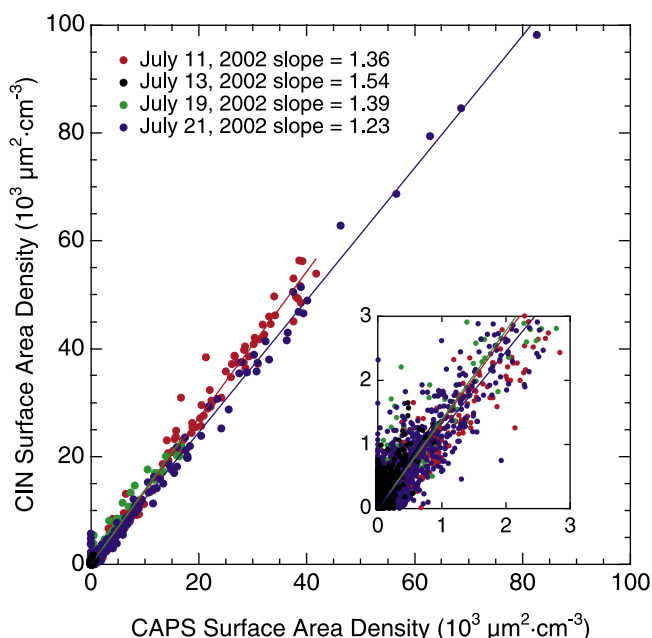


Figure 8. Comparison of CIN- and CAPS-derived SAD measured during the flights of 11, 13, 19, and 21 July 2002. Data at SADs less than $3 \mu\text{m}^2 \text{cm}^{-3}$ are expanded in the inset. All data are shown as 10-s averages. Lines represent a least squares fit to the data for each flight date. The slope of the linear fit (constrained through the origin) is shown for each flight date in the figure legend.

onboard the WB-57F during CRYSTAL-FACE. SAD was derived from the CAPS data by integrating particle size distribution and number density measurements, while bulk measurements of cloud extinction coefficient at 635 nm were used to derive SAD from the CIN data. A comparison between the CIN- and CAPS-derived SADs indicates good agreement between the two instruments for the flights on 11, 19, and 21 July, with SADs derived from the CIN measurements ranging from 23–39% higher than the CAPS-derived values on those 3 flight days (Figure 8). On 13 July the CIN measurements were 54% higher than the CAPS values, which may be attributable to the sampling of optically thin subvisual cirrus clouds near the tropopause on that day. Cloud extinction in these subvisual cirrus is close to the sensitivity threshold of the CIN. The observed differences are nonetheless within the combined uncertainties of the two instruments on all 4 flight days. The analyses presented here make use of SADs derived from the CAPS measurements. Owing to the fact that the SADs derived from the CIN measurements are 23–54% higher than the CAPS values, the SADs utilized here can be considered lower limits.

[17] As stated previously, the value of EF used in calculating $\text{HNO}_3|_{\text{con}}$ approaches a maximum value of U_0/U (the ratio of the WB-57F true air speed to the air velocity in the sample inlet) at particle sizes greater than approximately $10 \mu\text{m}$. SADs calculated from the CAPS measurements on the 4 flight days considered here (in cirrus clouds with total SADs greater than $200 \mu\text{m}^2 \text{cm}^{-3}$) indicate that $92 \pm 9\%$ of the surface area resides on particles larger than $10 \mu\text{m}$ in diameter. Use of the maximum value of EF in calculating $\text{HNO}_3|_{\text{con}}$ via equation (1), therefore, is expected

to introduce no more than 10% uncertainty into the value of $\text{HNO}_3|_{\text{con}}$.

[18] The VMD of cirrus cloud particles observed during CRYSTAL-FACE ranged from approximately $3 \mu\text{m}$ up to $700 \mu\text{m}$, with most clouds having VMDs greater than $20 \mu\text{m}$ (Figure 9a). The largest particles ($>500 \mu\text{m}$) were observed primarily in clouds with SADs greater than $10^4 \mu\text{m}^2 \text{cm}^{-3}$. As expected, IWC shows a strong correlation with SAD (Figure 9b). IWCs as high as 1000 ppmv were observed during some cloud events (Figure 9b). The highest values of VMD and IWC were observed from the WB-57F primarily at temperatures between 205 K and 215 K during the flights shown in Figure 9.

4. Discussion

4.1. HNO_3 Uptake on Cirrus Cloud Particles

[19] The coincident observation of cirrus clouds and condensed-phase HNO_3 during CRYSTAL-FACE is assumed here to result from the uptake of HNO_3 on the surface of cirrus cloud particles. Laboratory studies indicate that the low solubility of HNO_3 in ice will not allow a significant fraction of $\text{HNO}_3|_{\text{con}}$ to reside in the bulk of the cirrus particles [Sommerfeld *et al.*, 1998; Hanson and Ravishankara, 1991]. Furthermore, Dominé and Thibert [1996] have suggested that the high diffusivity of HNO_3 in ice is such that HNO_3 trapped in the bulk ice during particle formation will migrate to the particle surface. We note, however, that the measurements presented here cannot distinguish between surface uptake and HNO_3 that may be condensed in the bulk of the particles. HNO_3 uptake on cirrus cloud particles can be represented in terms of molecular coverage, given by the ratio of $\text{HNO}_3|_{\text{con}}$ to SAD in units of molecules cm^{-2} . HNO_3 surface coverages observed during CRYSTAL-FACE are shown as a function of temperature in Figure 10, with symbols colored according to $P(\text{HNO}_3)$ (see legend). Data shown by triangles at temperatures less than 200 K in Figure 10 represent observations under conditions in which nitric acid trihydrate (NAT) is stable, as predicted by ambient temperature and the ratio of $\text{HNO}_3|_{\text{gas}}$ to H_2O vapor [Hanson and Mauersberger, 1988; Gao *et al.*, 2003]. It has been proposed that, under conditions in which NAT is stable, HNO_3 forms NAT clusters or layers on the particle surface which interfere with the condensation of H_2O molecules on the particle surface, and thereby increase the relative humidity with respect to ice in the cirrus cloud [Gao *et al.*, 2003].

[20] The mean HNO_3 coverage observed during CRYSTAL-FACE was 1.9×10^{13} molecules cm^{-2} , with maximum coverages reaching 1.4×10^{14} molecules cm^{-2} during a few cirrus cloud events (Figure 10). While the greatest coverages were observed at temperatures between 205 K and 210 K, mean coverages binned according to temperature show no temperature dependence above 200 K (black symbols in Figure 10). The average value for measurements between 195 K and 200 K is approximately a factor of 3 greater than values above 200 K. Generally higher HNO_3 coverages at lower temperatures have been observed in field measurements reported by both Kondo *et al.* [2003] and Ziereis *et al.* [2004]. HNO_3 coverages show a minimal dependence on $P(\text{HNO}_3)$, with the lowest cover-

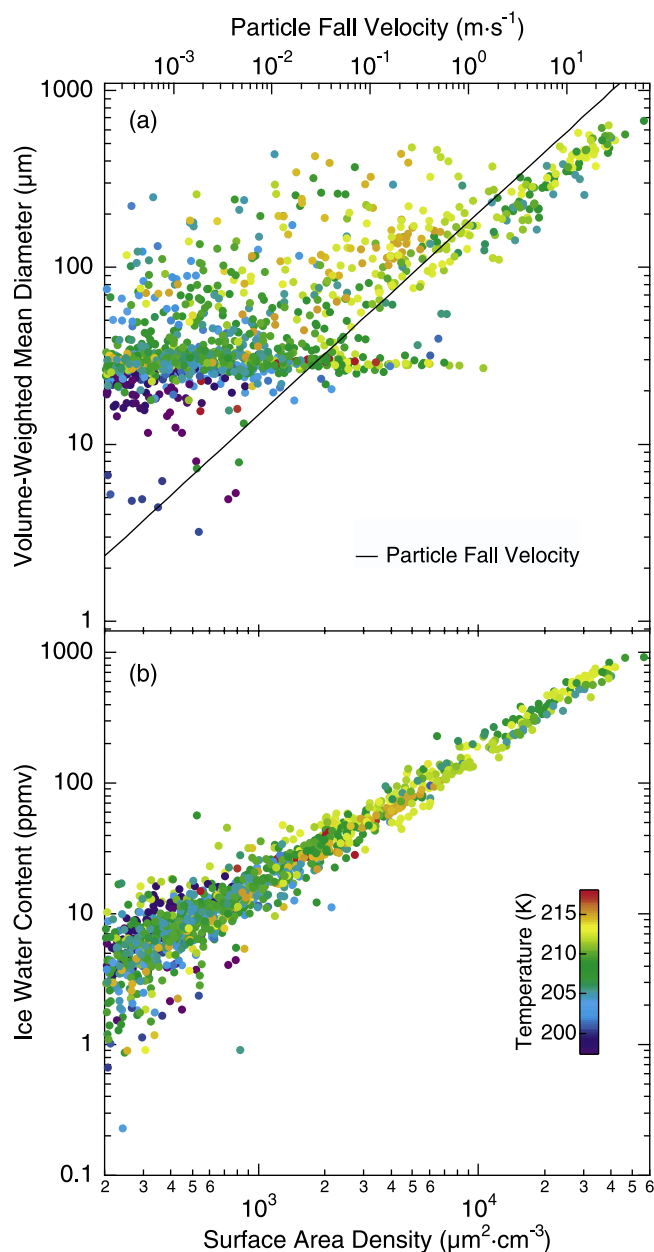


Figure 9. (a) Volume-weighted mean diameter of cirrus cloud particles versus SAD measured during the flights on 11, 13, 19, and 21 July 2002. Only data at SADs greater than $200 \mu\text{m}^2 \text{cm}^{-3}$ are shown. Data are colored according to ambient temperature. The black line represents the terminal fall velocity for ice particles in the upper troposphere, calculated according to Meier and Hendricks [2002]. (b) IWC (represented as a gas-phase equivalent volume mixing ratio) versus SAD. At 130 hPa and 200 K, an IWC of 100 ppmv is equivalent to an ice water concentration of 14 mg m^{-3} . Other details same as Figure 9a.

ages occurring at $P(\text{HNO}_3)$ values below 2.5×10^{-8} hPa (Figure 10). A number of laboratory studies have also reported increased HNO_3 coverages with increasing $P(\text{HNO}_3)$, albeit at $P(\text{HNO}_3)$ values substantially higher than those presented here (5.0×10^{-7} to 3.0×10^{-6} hPa) [Hudson et al., 2002; Hynes et al., 2002]. These results

highlight the need for a comprehensive laboratory study of HNO_3 uptake on ice surfaces at $P(\text{HNO}_3)$ values below 2.0×10^{-7} hPa that are typical of the subtropical UT.

[21] The coverage of HNO_3 on ice, in general, can be modeled or predicted using the kinetics or thermodynamics of the uptake process [Gao et al., 2003; Hudson et al., 2002]. Using laboratory measurements and a semiempirical equilibrium surface coverage model, Hudson et al. [2002] have predicted HNO_3 coverage on ice surfaces as a function of temperature and $P(\text{HNO}_3)$. This multilayer Frenkel-Halsey-Hill (FHH) model was fitted to equilibrium HNO_3 coverages observed on vapor-deposited ice films at temperatures between 213 K and 219 K with a $P(\text{HNO}_3)$ of 1.1×10^{-6} hPa. HNO_3 surface coverages predicted by the FHH model are shown as a function of temperature in Figure 11a, together with the HNO_3 coverages observed in cirrus clouds during CRYSTAL-FACE. The isobaric lines representing the modeled coverages are colored on the same scale as the observed coverages according to the values of $P(\text{HNO}_3)$ input to the model. Figure 11a indicates better agreement between the modeled and observed HNO_3 coverages at temperatures higher than approximately 205 K, while at lower temperatures the modeled coverages increase to values far greater than those observed at comparable temperatures and $P(\text{HNO}_3)$ values. The high model coverages

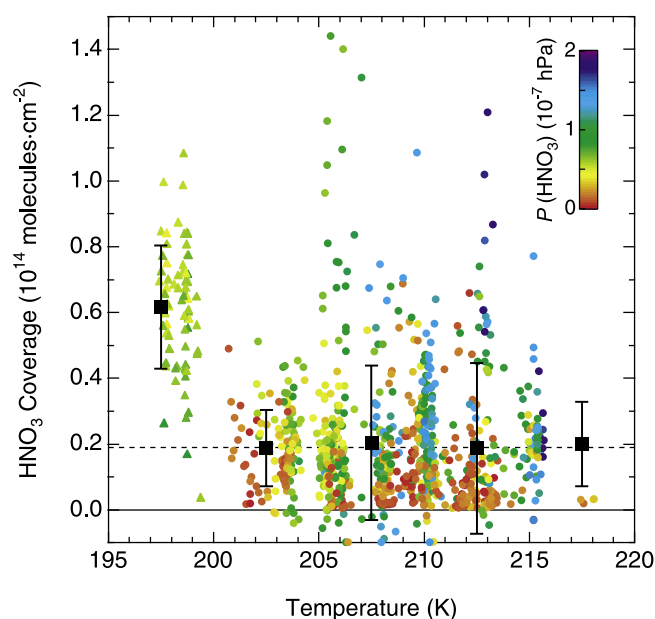


Figure 10. HNO_3 coverage versus temperature for measurements made in cirrus clouds at SADs greater than $200 \mu\text{m}^2 \text{cm}^{-3}$ on 11, 13, 19, and 21 July 2002. Symbols are colored according to $P(\text{HNO}_3)$. Triangles at temperatures less than 200 K indicate measurements made under conditions in which NAT is stable. Mean values of HNO_3 coverage are plotted as the mean of 5 K temperature bins from 195 to 220 K (black squares). Error bars represent the standard deviation in each temperature bin. Negative values of HNO_3 coverage are included in the calculation of the mean values. The dashed line at $1.9 \times 10^{13} \text{ molecules cm}^{-2}$ represents the mean HNO_3 coverage observed during CRYSTAL-FACE. A complete HNO_3 monolayer is formed when the coverage reaches $1.0 \times 10^{15} \text{ molecules cm}^{-2}$.

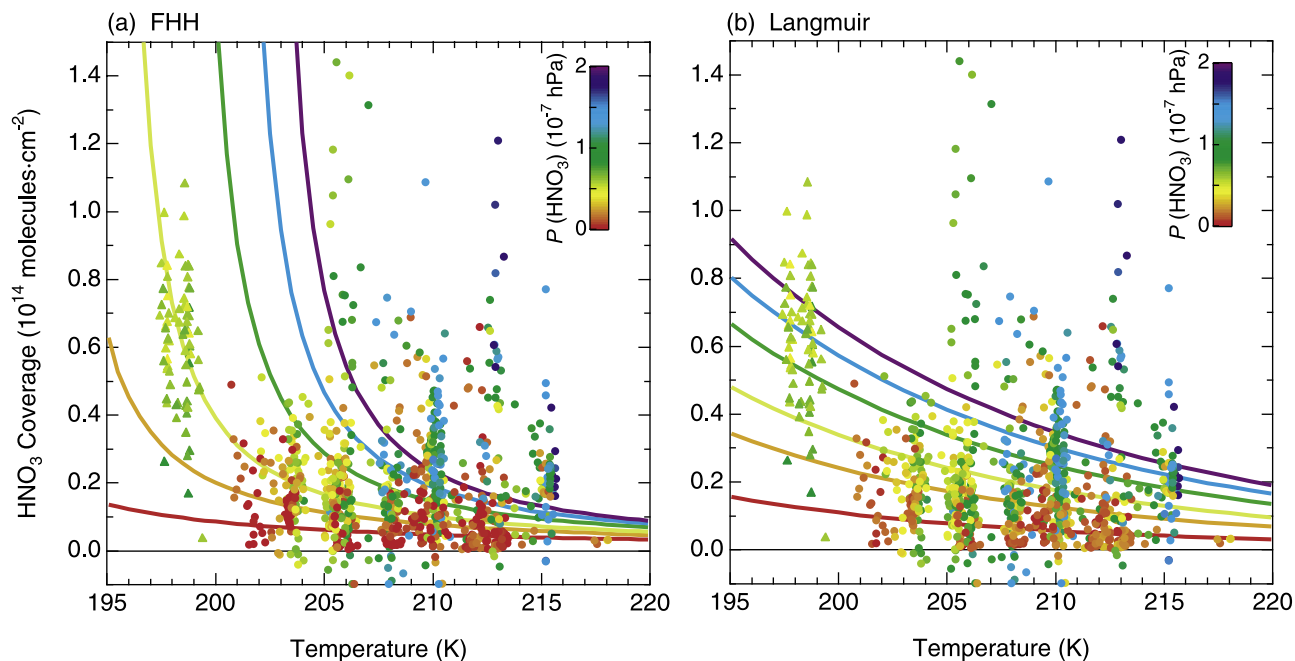


Figure 11. HNO_3 coverage versus temperature for measurements made in cirrus clouds at SADs greater than $200 \mu\text{m}^2 \text{cm}^{-3}$ on 11, 13, 19, and 21 July 2002. Symbols are colored according to $P(\text{HNO}_3)$. Triangles at temperatures less than 200 K indicate measurements made under conditions in which NAT is stable. Data are represented as 10-s averages. (a) Lines are isobars representing HNO_3 coverages calculated by the FHH HNO_3 uptake model [Hudson *et al.*, 2002] and are colored according to the same temperature scale as the observed coverages (see legend). (b) Same as Figure 11a, except the isobars represent HNO_3 coverages calculated by the Langmuir surface chemistry model.

below 205 K may result from the fact that the model was fitted to laboratory data at temperatures above 213 K, and the coverages presented here, therefore, are extrapolated to lower temperatures where the uncertainty in the model increases.

[22] A number of studies have described the uptake of HNO_3 on ice surfaces using a Langmuir surface chemistry model [Tabazadeh *et al.*, 1999; Hynes *et al.*, 2002; Meier and Hendricks, 2002]. The Langmuir isotherm predicts the fractional HNO_3 surface coverage (θ) according to equation (2),

$$\theta = \frac{K_{eq}^{1/2} \cdot P(\text{HNO}_3)^{1/2}}{1 + K_{eq}^{1/2} \cdot P(\text{HNO}_3)^{1/2}}, \quad (2)$$

where K_{eq} represents the equilibrium adsorption constant, given by the ratio of the rates of adsorption and desorption (k_a/k_d) [Laidler and Meiser, 1982]. The value of θ is unity when the HNO_3 surface coverage reaches a complete monolayer ($1.0 \times 10^{15} \text{ molecules cm}^{-2}$). We note that the surface density of HNO_3 molecules when forming a complete monolayer is somewhat uncertain, and the density of $1.0 \times 10^{15} \text{ molecules cm}^{-2}$ stated here should be considered an upper limit [Hudson *et al.*, 2002]. If the HNO_3 surface density is lower than $1.0 \times 10^{15} \text{ molecules cm}^{-2}$ for a complete monolayer, the resulting fractional surface coverages will be higher than those stated here. Application of the dissociative form of the Langmuir isotherm is supported here by spectroscopic studies of HNO_3 uptake on thin ice films at 211 K, which indicate, by the presence of H_3O^+ and NO_3^- ions on the ice surface, that HNO_3

dissociates upon adsorption [Zondlo *et al.*, 1997]. The temperature-dependent equilibrium adsorption constant in equation (2) can be calculated according to equation (3) [Adamson and Gast, 1997],

$$K_{eq} = \frac{100 \cdot N_A \cdot \sigma_0 \cdot \tau_0}{(2\pi \cdot M \cdot R \cdot T)^{1/2}} e^{\left(\frac{-\Delta H_{ads}}{c \cdot R \cdot T}\right)} \text{ hPa}^{-1}, \quad (3)$$

where N_A is Avogadro's number ($6.02 \times 10^{23} \text{ mol}^{-1}$), σ_0 is the area of one adsorption site (10^{-19} m^2), τ_0 is the time constant for adsorbate oscillation perpendicular to the surface (10^{-13} s), M is the molecular weight of HNO_3 ($0.063 \text{ kg mol}^{-1}$), R is the ideal gas constant ($8.314 \text{ J mol}^{-1} \text{ K}^{-1}$), T is temperature (in K), c is a unit conversion factor ($2.39 \times 10^{-4} \text{ kcal J}^{-1}$) and ΔH_{ads} is the adsorption enthalpy of HNO_3 on ice (in kcal mol^{-1}).

[23] Using equations (2) and (3), a Langmuir isotherm was fitted to the CRYSTAL-FACE observations of fractional surface coverage and $P(\text{HNO}_3)$ (Figure 12). Using the median temperature of 208 K for the observations shown in Figure 9, the best fit to the experimental data was achieved with a ΔH_{ads} of $-11.0 \text{ kcal mol}^{-1}$, or 46.0 kJ mol^{-1} (red line in Figure 12). Note that the data are largely bound by ΔH_{ads} values of $-10.0 \text{ kcal mol}^{-1}$ and $-12.0 \text{ kcal mol}^{-1}$. Also shown in Figure 12 are Langmuir isotherms at the same temperature for ΔH_{ads} values of $-14.2 \text{ kcal mol}^{-1}$ and $-12.9 \text{ kcal mol}^{-1}$ reported by Tabazadeh *et al.* [1999] and Hynes *et al.* [2002], respectively. Fractional coverages predicted using these previously published values of ΔH_{ads} far exceed the coverages observed during CRYSTAL-FACE,

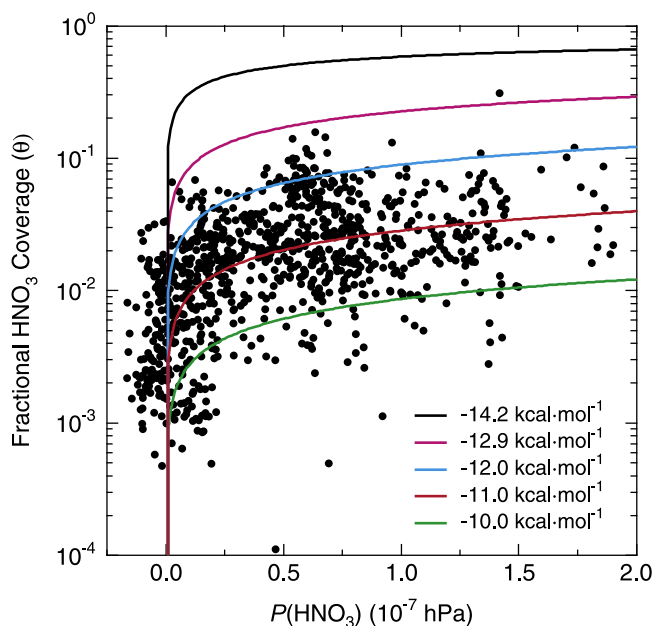


Figure 12. Fractional HNO_3 surface coverage (θ) versus $P(\text{HNO}_3)$ measured during the flights of 11, 13, 19, and 21 July 2002. Colored lines are isotherms fitted according to equations (2) and (3) (see text) with values of ΔH_{ads} shown in the legend and the median observed temperature of 208 K. All data are represented as 10-s averages for measurements made at SADs greater than $200 \mu\text{m}^2 \text{cm}^{-3}$.

indicating these adsorption enthalpies are too high to accurately describe the observations presented here. Bartels-Rausch *et al.* [2002], using a chromatographic technique, have recently reported a ΔH_{ads} for HNO_3 uptake on ice of $-10.5 \text{ kcal mol}^{-1}$ that is in good agreement with the value of $-11.0 \text{ kcal mol}^{-1}$ presented here. We caution that the effective ΔH_{ads} reported here is empirically derived from observations in a dynamic system which may or may not be in steady state, and this value, therefore, cannot be considered a fundamental thermodynamic parameter. Nonetheless, the Langmuir formalism, using a ΔH_{ads} of $-11.0 \text{ kcal mol}^{-1}$, effectively describes the CRYSTAL-FACE observations of HNO_3 uptake on cirrus cloud particles to within a factor of 5 (Figure 12). It should be noted that the data shown in Figure 12 span a temperature range from 197 K to 218 K, and that the Langmuir isotherms were fitted at the median temperature of 208 K. Use of a single temperature in fitting the isotherms is supported by the results of Hynes *et al.* [2002], who reported a variation of less than 2% between values of ΔH_{ads} derived from laboratory measurements at 218 K and 228 K.

[24] Having derived an effective value of ΔH_{ads} for HNO_3 adsorption on cirrus cloud particles in the UT, HNO_3 coverages predicted by the Langmuir surface chemistry model (as a function of temperature) can be compared to the CRYSTAL-FACE observations (Figure 11b). As in Figure 11a, the isobaric lines are colored on the same scale as the observed coverages. The calculated coverages shown in Figure 11b indicate that the model does not adequately describe the considerable variability in the observed coverages at a given temperature and $P(\text{HNO}_3)$.

Nonetheless, when using the empirically derived ΔH_{ads} of $-11.0 \text{ kcal mol}^{-1}$, the Langmuir model is capable of predicting the observed coverages within a factor of 5 or better. The variability in the observed coverages, and the less than perfect agreement with the uptake models, can be explained, in part, if the adsorbed HNO_3 is not in equilibrium with HNO_3 in the gas phase. Previous field studies have also shown HNO_3 surface coverages to be highly variable throughout the temperature and $P(\text{HNO}_3)$ ranges observed [Kondo *et al.*, 2003; Ziereis *et al.*, 2004].

4.2. HNO_3 Partitioning in Cirrus Clouds

[25] The fraction of total HNO_3 present on cirrus cloud particles was observed to increase with SAD during CRYSTAL-FACE (Figure 13). The mean value of HNO_3 partitioned in the condensed phase at SADs greater than $200 \mu\text{m}^2 \text{cm}^{-3}$ was 16%. Up to 100% of the total HNO_3 was partitioned on ice particles during some cirrus cloud encounters, at SADs between 350 and $4.2 \times 10^4 \mu\text{m}^2 \text{cm}^{-3}$ and temperatures between 201 K and 213 K. Measurements reported by Ziereis *et al.* [2004] in midlatitude cirrus clouds reveal a similar relationship between condensed-phase NO_y partitioning and SAD, although maximum reported values of

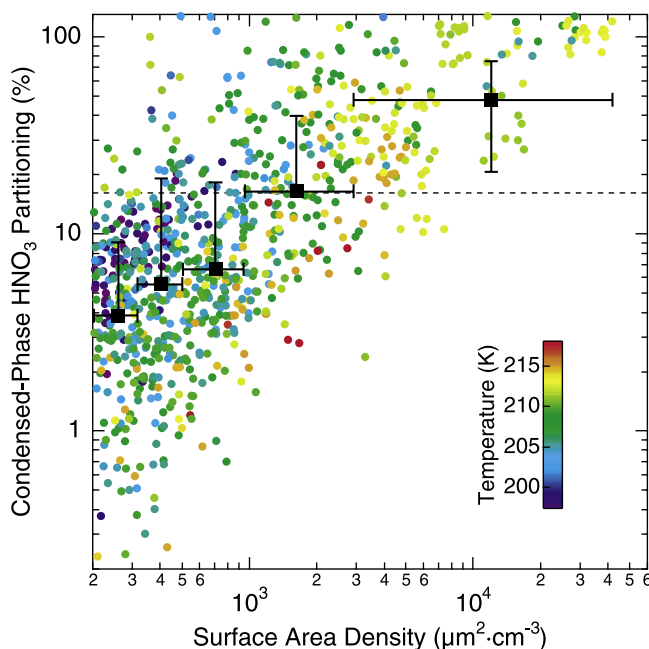


Figure 13. Fraction of total HNO_3 in the condensed phase versus SAD measured during the flights of 11, 13, 19, and 21 July 2002. Data are represented as 10-s averages for measurements made at SADs greater than $200 \mu\text{m}^2 \text{cm}^{-3}$ and are colored according to temperature. Black squares represent mean values of the 10-s data grouped into quintiles. Vertical bars represent the standard deviation about the mean value in each quintile and horizontal bars represent the upper and lower boundaries of each quintile. Values of condensed-phase partitioning greater than 100% occur when zero or near-zero $\text{HNO}_3|_{\text{gas}}$ abundances are measured as negative values. The dashed line at 16% represents the mean value of HNO_3 partitioned in the condensed phase during CRYSTAL-FACE.

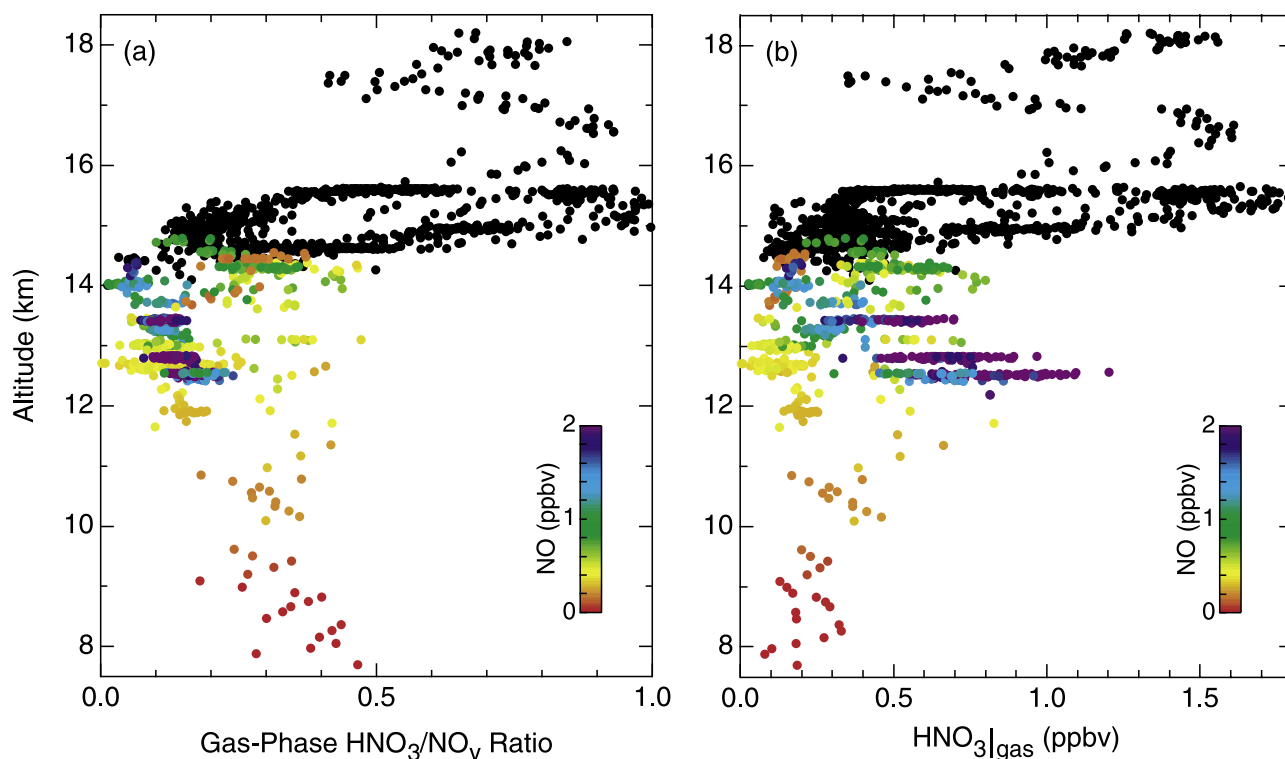


Figure 14. (a) Vertical profile of the gas-phase HNO_3/NO_y ratio observed in cloud free air (SADs less than $20 \mu\text{m}^2 \text{cm}^{-3}$) during the flights of 11, 13, 19, and 21 July 2002. Tropospheric measurements (according to the Microwave Temperature Profiler) are colored according to measured NO. Stratospheric measurements are shown in black. (b) Vertical profile of $\text{HNO}_3|_{\text{gas}}$. Other details same as Figure 14a.

condensed-phase NO_y partitioned in cirrus clouds did not exceed 50% of the total observed NO_y . Measurements of NO_y uptake in a mountain wave cirrus cloud reported by Weinheimer *et al.* [1998] indicate complete uptake of HNO_3 , provided that the ambient HNO_3/NO_y ratio in the cloud was 0.1–0.2. Gas-phase HNO_3 was not measured in either of these previous studies, making an accurate assessment of the fraction of HNO_3 remaining in the gas phase after uptake difficult.

[26] Krämer *et al.* [2003] have recently studied the partitioning of HNO_3 in Arctic cirrus clouds, and have modeled the role of HNO_3 uptake by interstitial $\text{HNO}_3\text{-H}_2\text{SO}_4\text{-H}_2\text{O}$ ternary solution aerosols in partitioning. This study concluded that some fraction of the total HNO_3 in Arctic cirrus clouds must remain in the gas phase, with the remainder partitioned predominately in interstitial aerosols at temperatures less than 205 K when SADs are low, and on cirrus cloud particles at higher SADs. Measurements in subtropical cirrus clouds reported here, however, indicate that up to 100% of the total HNO_3 can be partitioned in cirrus ice particles both at low temperatures and low SADs. Furthermore, we see no evidence of significant uptake of HNO_3 in ternary solution aerosols outside of clouds in the subtropical UT during the flights considered in this study. There is evidence, however, of HNO_3 uptake by ternary solution aerosols in the near absence of cirrus ice particles on at least one other CRYSTAL-FACE flight (9 July 2002) (A. J. Weinheimer *et al.*, manuscript in preparation, 2004). We also note that HNO_3 may be

contained in a ternary solution on the surface of the cirrus ice particles.

4.3. HNO_3 and HNO_3/NO_y in the Cloud-Free Upper Troposphere and Lower Stratosphere

[27] Measurements in the cloud-free subtropical UT during CRYSTAL-FACE indicate that the gas-phase HNO_3/NO_y ratio is highly variable, ranging from zero to approximately 0.5 (colored symbols in Figure 14a). The HNO_3/NO_y ratio is generally higher and also variable in the subtropical lower stratosphere (LS), with values observed between 0.05 and 1 (black symbols in Figure 14a). HNO_3 is expected to be the predominate NO_y species in the LS away from the tropopause region [Neuman *et al.*, 2001]. The lower HNO_3/NO_y ratios (<0.3) observed in the UT are affected by low observed values of HNO_3 , due to HNO_3 removal by uptake and sedimentation by cloud particles in cirrus processed air masses (yellow symbols in Figure 14b), or from elevated levels of NO_y due to NO production from lightning strikes (purple symbols in Figure 14b). Previously measured values of the HNO_3/NO_y ratio in the midlatitude UT over the continental United States were also highly variable and ranged from approximately 0.1 to 0.5 [Neuman *et al.*, 2001]. The large range and variability of HNO_3/NO_y ratios observed in the UT during CRYSTAL-FACE highlights the value in measuring gas-phase HNO_3 when assessing HNO_3 uptake on cirrus cloud particles, over deriving gas-phase HNO_3 from measured NO_y and a constant assumed HNO_3/NO_y ratio.

[28] A number of cirrus clouds observed in the subtropical UT during CRYSTAL-FACE had VMDs between 200 μm and 700 μm . Terminal fall velocities for cirrus ice particles in this size range are 1 m s^{-1} to 10 m s^{-1} (Figure 9a) [Meier and Hendricks, 2002]. With 16% of the total HNO_3 in cirrus clouds adsorbed on ice particles, the gravitational redistribution of a significant fraction of the total HNO_3 in these clouds can therefore occur on a timescale of minutes to hours. Cirrus clouds with up to 100% of the total HNO_3 partitioned in the condensed phase have even greater potential to redistribute HNO_3 in the UT.

5. Conclusions and Implications

[29] A number of cirrus cloud encounters in the UT by the NASA WB-57F during CRYSTAL-FACE were accompanied by the observation of condensed-phase HNO_3 . Maximum levels of condensed-phase HNO_3 exceeded the gas-phase equivalent of 0.8 ppbv during some cirrus events. A mean HNO_3 surface coverage of 1.9×10^{13} molecules cm^{-2} was observed on the flights of 11, 13, 19, and 21 July 2002, with maximum surface coverages reaching as high as 1.4×10^{14} molecules cm^{-2} during a few cirrus cloud encounters. Molecular coverages predicted using a Langmuir surface chemistry model agree with the observed coverages to within a factor of 5 or better when using an empirically derived ΔH_{ads} of -11.0 kcal mol^{-1} . The mean percentage of total HNO_3 condensed on cirrus cloud particles was 16%, with up to 100% of the HNO_3 partitioned in the condensed phase in a number of cirrus clouds. The fraction of total HNO_3 in the condensed phase was found to increase strongly with SAD. Based on the large diameters of cloud particles containing HNO_3 observed during CRYSTAL-FACE, the redistribution of HNO_3 in the UT will be very effective in some cloud systems. The interpretation of future observations of HNO_3 uptake on cirrus particles will be improved by a knowledge of the individual history of the air parcels in which the cirrus clouds are formed [Kärcher, 2003] and laboratory studies of HNO_3 uptake at low gas-phase abundances ($P(\text{HNO}_3) < 2.0 \times 10^{-7}$ hPa) and low temperatures (195 K–220 K).

[30] **Acknowledgments.** The authors wish to thank the air and ground crews of the NASA WB-57F aircraft. Helpful discussions with J. P. D. Abbatt, E. R. Lovejoy, and H. Ziereis are also appreciated. This work was partially supported by the National Aeronautics and Space Administration Upper Atmospheric Research Program and Radiation Science Program. Work done by MJM at the Jet Propulsion Laboratory, California Institute of Technology, was carried out under contract with the National Aeronautics and Space Administration.

References

- Abbatt, J. P. D. (1997), Interaction of HNO_3 with water-ice surfaces at temperatures of the free troposphere, *Geophys. Res. Lett.*, **24**(12), 1479–1482.
- Adamson, A. W., and A. P. Gast (1997), *Physical Chemistry of Surfaces*, 6th Ed., John Wiley, New York.
- Albritton, D. L., et al. (2001), Technical summary of the Working Group I report, in *Climate Change 2001: The Scientific Basis. Contribution of Working Group I to the Third Assessment Report of the Intergovernmental Panel on Climate Change*, edited by J. T. Houghton et al., pp. 21–83, Cambridge Univ. Press, New York.
- Arora, O. P., et al. (1999), Uptake of nitric acid by sub-micron-sized ice particles, *Geophys. Res. Lett.*, **26**(24), 3621–3624.
- Bartels-Rausch, T., et al. (2002), The adsorption enthalpy of nitrogen oxides on crystalline ice, *Atmos. Chem. Phys.*, **2**, 235–247.
- Baumgardner, D., et al. (2001), The cloud, aerosol and precipitation spectrometer: A new instrument for cloud investigations, *Atmos. Res.*, **59**–60, 251–264.
- Denning, R. F., S. L. Guidero, G. S. Parks, and B. L. Gary (1989), Instrument description of the Airborne Microwave Temperature Profiler, *J. Geophys. Res.*, **94**, 16,757–16,765.
- Domine, F., and E. Thibert (1996), Mechanism of incorporation of trace gases in ice grown from the gas phase, *Geophys. Res. Lett.*, **23**(24), 3627–3630.
- Gao, R. S., et al. (2003), Evidence that ambient nitric acid increases relative humidity in low-temperature cirrus clouds, *Science*, in press.
- Gerber, H., Y. Takano, T. J. Garrett, and P. V. Hobbs (2000), Nephelometer measurements of the asymmetry parameter, volume extinction coefficient, and backscatter ratio in arctic clouds, *J. Atmos. Sci.*, **57**, 3021–3034.
- Hanson, D., and K. Mauersberger (1988), Laboratory studies of the nitric acid trihydrate: Implications for the south polar stratosphere, *Geophys. Res. Lett.*, **15**(8), 855–858.
- Hanson, D., and A. R. Ravishankara (1991), The reaction probabilities of ClONO_2 and N_2O_5 on polar stratospheric cloud materials, *J. Geophys. Res.*, **96**(3), 5081–5090.
- Heymsfield, A. J., and G. M. McFarquhar (2002), Mid-latitude and tropical cirrus: Microphysical properties, in *Cirrus*, edited by D. K. Lynch et al., pp. 78–101, Oxford Univ. Press, New York.
- Hudson, P. K., et al. (2002), Uptake of nitric acid on ice at tropospheric temperatures: Implications for cirrus clouds, *J. Phys. Chem. A*, **106**, 9874–9882.
- Hynes, R. G., M. A. Fernandez, and R. A. Cox (2002), Uptake of HNO_3 on water-ice and coadsorption of HNO_3 and HCl in the temperature range 210–235 K, *J. Geophys. Res.*, **107**(D24), 4797, doi:10.1029/2001JC001557.
- Jaeglé, L., et al. (1998), Sources of HO_x and production of ozone in the upper troposphere over the United States, *Geophys. Res. Lett.*, **25**(10), 1709–1712.
- Jin, Y., W. B. Rossow, and D. P. Wylie (1996), Comparison of the climatologies of high-level clouds from HIRS and ISCCP, *J. Clim.*, **9**, 2850–2879.
- Kärcher, B. (2002), Properties of subvisible cirrus clouds formed by homogeneous freezing, *Atmos. Chem. Phys.*, **2**, 161–170.
- Kärcher, B. (2003), Simulating gas-aerosol-cirrus interactions: Process-oriented microphysical model and applications, *Atmos. Chem. Phys.*, **3**, 1645–1664.
- Kondo, Y., et al. (2003), Uptake of reactive nitrogen on cirrus cloud particles in the upper troposphere and lowermost stratosphere, *Geophys. Res. Lett.*, **30**(4), 1154, doi:10.1029/2002GL016539.
- Krämer, M., et al. (2003), Nitric acid partitioning in cirrus clouds: A synopsis based on field, laboratory and model studies, *Atmos. Chem. Phys. Discuss.*, **3**, 413–443.
- Lacis, A. A., D. J. Wuebbles, and J. A. Logan (1990), Radiative forcing of climate by changes in the vertical distribution of ozone, *J. Geophys. Res.*, **95**(D7), 9971–9982.
- Laidler, K. J., and J. H. Meiser (1982), *Physical Chemistry*, Benjamin-Cummings, Menlo Park, Calif.
- Lawrence, M. G., and P. J. Crutzen (1998), The impact of cloud particle gravitational settling on soluble trace gas distributions, *Tellus, Ser. B*, **50**, 263–289.
- Liao, X., W. B. Rossow, and D. Rind (1995), Comparison between SAGE II and ISCCP high-level clouds: 1. Global and zonal mean cloud amounts, *J. Geophys. Res.*, **100**(D1), 1121–1135.
- Liou, K.-N. (1986), Influence of cirrus clouds on weather and climate processes: A global perspective, *Mon. Weather Rev.*, **114**, 1167–1199.
- Lynch, D. K. (2002), Cirrus history and definition, in *Cirrus*, edited by D. K. Lynch et al., pp. 3–10, Oxford Univ. Press, New York.
- Meier, A., and J. Hendricks (2002), Model studies on the sensitivity of upper tropospheric chemistry to heterogeneous uptake of HNO_3 on cirrus ice particles, *J. Geophys. Res.*, **107**(D23), 4696, doi:10.1029/2001JD000735.
- Meilinger, S. K., et al. (1999), HNO_3 partitioning in cirrus clouds, *Geophys. Res. Lett.*, **26**(14), 2207–2210.
- Neuman, J. A., et al. (1999), Study of inlet materials for sampling atmospheric nitric acid, *Environ. Sci. Technol.*, **33**, 1133–1136.
- Neuman, J. A., et al. (2000), A fast-response chemical ionization mass spectrometer for in situ measurements of HNO_3 in the upper troposphere and lower stratosphere, *Rev. Sci. Instrum.*, **71**(10), 3886–3892.
- Neuman, J. A., et al. (2001), In situ measurements of HNO_3 , NO_y , NO , and O_3 in the lower stratosphere and upper troposphere, *Atmos. Environ.*, **35**, 5789–5797.
- Northway, M. J., et al. (2002), An analysis of large HNO_3 -containing particles sampled in the Arctic stratosphere during the winter of 1999/2000, *J. Geophys. Res.*, **107**(D20), 8298, doi:10.1029/2001JD001079.

- Sassen, K. (2002), Cirrus clouds: A modern perspective, in *Cirrus*, edited by D. K. Lynch et al., pp. 11–40, Oxford Univ. Press, New York.
- Scott, S. G., T. P. Bui, K. R. Chan, and S. W. Bowen (1990), The meteorological measurement system on the NASA ER-2 aircraft, *J. Atmos. Oceanic Technol.*, 7, 525–540.
- Sommerfeld, R. A., C. A. Knight, and S. K. Laird (1998), Diffusion of HNO_3 in ice, *Geophys. Res. Lett.*, 25(6), 935–938.
- Tabazadeh, A., O. B. Toon, and E. J. Jensen (1999), A surface chemistry model for nonreactive trace gas adsorption on ice: Implications for nitric acid scavenging by cirrus, *Geophys. Res. Lett.*, 26(14), 2211–2214.
- Vincent, J. H., et al. (1986), On the aspiration characteristics of large-diameter thin-walled aerosol sampling probes at yaw orientations with respect to the wind, *J. Aerosol Sci.*, 17(2), 211–224.
- Wang, P.-H., et al. (1996), A 6-year climatology of cloud occurrence frequency from Stratospheric Aerosol and Gas Experiment II observations (1985–1990), *J. Geophys. Res.*, 101(D23), 29,407–29,429.
- Weinheimer, A. J., et al. (1998), Uptake of NO_y on wave-cloud ice particles, *Geophys. Res. Lett.*, 25(10), 1725–1728.
- Weinstock, E. M., et al. (1994), New fast-response photofragment fluorescence hygrometer for use on the NASA ER-2 and the Perseus remotely piloted aircraft, *Rev. Sci. Instrum.*, 65(11), 3544–3554.
- Wylie, D. P., and W. P. Menzel (1999), Eight years of high cloud statistics using HIRS, *J. Clim.*, 12, 170–184.
- Ziereis, H., et al. (2004), Uptake of reactive nitrogen on cirrus cloud particles during INCA, *Geophys. Res. Lett.*, 31, doi:10.1029/2003GL018794, in press.
- Zondlo, M. A., S. B. Barone, and M. A. Tolbert (1997), Uptake of HNO_3 on ice under upper tropospheric conditions, *Geophys. Res. Lett.*, 24(11), 1391–1394.
-
- D. Baumgardner, Universidad Nacional Autonoma de Mexico, Centro de Ciencias de la Atmosfera, Ciudad Universitaria, 04510 Mexico DF, Mexico.
- T. P. Bui, NASA Ames Research Center, Moffett Field, CA 94035, USA.
- S. Dhaniyala, Department of Mechanical and Aeronautical Engineering, Clarkson University, Potsdam, NY 13699, USA.
- D. W. Fahey, R. S. Gao, P. K. Hudson, T. P. Marcy, P. J. Popp, and T. L. Thompson, Aeronomy Laboratory, National Oceanic and Atmospheric Administration, Boulder, CO 80305, USA. (ppopp@al.noaa.gov)
- T. J. Garrett, Department of Meteorology, University of Utah, Salt Lake City, UT 84112, USA.
- B. Kärcher, DLR, Institut für Physik der Atmosphäre, D-82234 Wessling, Germany.
- D. J. Knapp, D. D. Montzka, B. A. Ridley, and A. J. Weinheimer, Atmospheric Chemistry Division, National Center for Atmospheric Research, Boulder, CO 80307, USA.
- M. J. Mahoney, Jet Propulsion Laboratory, California Institute of Technology, Pasadena, CA 91109, USA.
- J. V. Pittman, D. S. Sayres, J. B. Smith, and E. M. Weinstock, Atmospheric Research Project, Harvard University, Cambridge, MA 02138, USA.